IEEE Photonics Journal
An IEEE Photonics Society Publication

Open Access

Multiple Fano Resonances Based on Different Waveguide Modes in a Symmetry Breaking Plasmonic System

Volume 6, Number 6, December 2014

Zhao Chen
Li Yu

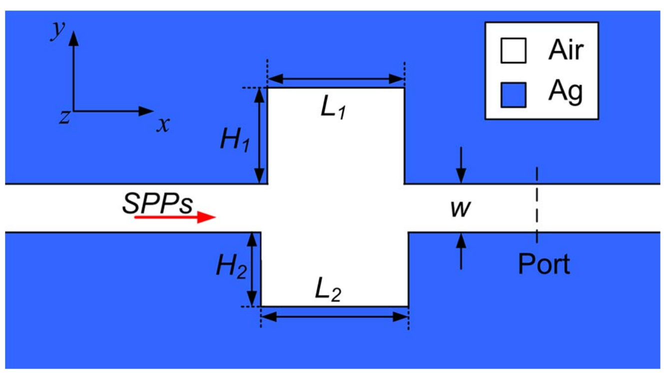

DOI: 10.1109/JPHOT.2014.2368779

Multiple Fano Resonances Based on Different Waveguide Modes in a Symmetry Breaking Plasmonic System

Zhao Chen and Li Yu

State Key Laboratory of Information Photonics and Optical Communications, Beijing University of Posts and Telecommunications, Beijing 100876, China
School of Science, Beijing University of Posts and Telecommunications, Beijing, 100876, China

DOI: 10.1109/JPHOT.2014.2368779

Manuscript received September 24, 2014; revised November 2, 2014; accepted November 4, 2014. Date of publication November 10, 2014; date of current version December 2, 2014. This work was supported in part by the National Natural Science Foundation of China under Grant 11374041, by the National Basic Research Program of China under Grant 2010CB923202, and by the Fund of State Key Laboratory of Information Photonics and Optical Communications, Beijing University of Posts and Telecommunications, China. Corresponding author: L. Yu (e-mail: bupt.yuli@gmail.com).

Abstract: Multiple Fano resonances are numerically investigated based on different waveguide modes in a nanoscale plasmonic waveguide resonator system, which consists of two grooves coupled with a metal–insulator–metal (MIM) waveguide. Simulation results show that by introducing a small structural breaking in the plasmonic resonator, both symmetric and antisymmetric waveguide modes can be excited. Due to the interaction of the symmetric and antisymmetric waveguide modes, the transmission spectra possess a sharp asymmetrical profile. Because of different origins, these Fano resonances exhibit different dependence on the parameters of the structure and can be easily tuned. These characteristics offer flexibility to design the device. This nanosensor yields a sensitivity of ~820 nm/RIU and a figure-of-merit of $\sim 3.2 \times 10^5$. The utilization of the antisymmetric mode in the MIM waveguide provides a new possibility for designing high-performance plasmonic devices.

Index Terms: Surface plasmons, Fano resonance, resonator, sensor.

1. Introduction

Fano resonances have been studied extensively in quantum systems, and were realized well in plasmonic nanostructures in recent years. These resonances usually arise from the coupling and interference of a non-radiative mode and a continuum of radiative electromagnetic waves and are distinguished from the Lorentzian like profile by a distinctive asymmetric line shape [1], [2]. They have been observed in various plasmonic structures, such as nanoshells [3]–[5], rings [6]–[9], polymers [10]–[13] and metal–insulator–metal (MIM) waveguide [14]–[18]. Due to the advantage for enhanced bio-chemical sensing, spectroscopy, and multicolor nonlinear processes, the multiple Fano resonances become more important and have gained much attention [19]–[23]. Among all the nanostructures, the MIM waveguide structures have attracted many researchers attention because these structures exhibiting more suitable for the highly integrated optical circuits due to their deep-sub-wavelength confinement of light [24]–[27]. In the MIM waveguide, both of the symmetric and anti-symmetric waveguide modes could always be supported without modal cutoff in the visible and near-infrared wavelength ranges [28], [29]. The

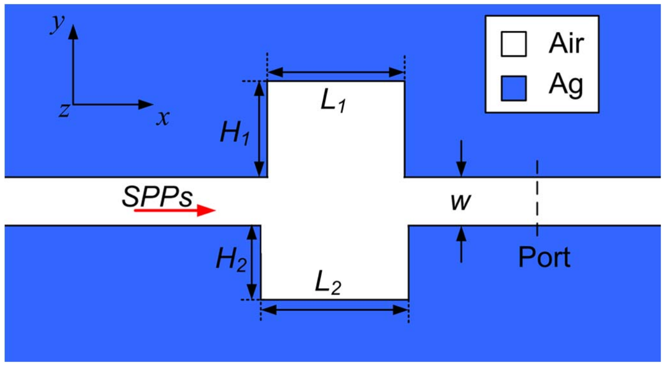

Fig. 1. Schematic configuration and geometric parameters of the plasmonic waveguide system.

symmetric waveguide mode in the MIM waveguide has long propagation lengths ($> 10\ \mu$m) [28], and thus, it was widely used in the ultra-small plasmonic devices [14]–[27], while the anti-symmetric waveguide mode in the MIM waveguide was hardly used in the SPP devices, especially in the MIM-based resonators. This is mainly attributed to its large propagation loss (propagation length $\sim$10 nm) [28] and its critical excitation condition [30]. In our previous work [31], we first introduced a metallic baffle in the wide gap resonator to excite the anti-symmetric mode, but the small baffle is difficult to fabricate due to the process technology, and only one Fano resonance profile was achieved.

In this paper, a MIM waveguide coupled with two different grooves is proposed to generate multiple Fano resonances. Simulation results show that by introducing a small structural breaking in the plasmonic resonator, both symmetric and anti-symmetric waveguide modes can be excited. Due to the interaction of the symmetric and anti-symmetric waveguide modes, the transmission spectra possess a sharp asymmetrical profile. Because of different origins, these Fano resonances exhibit different dependence on the parameters of the structure, and can be easily tuned. The proposed sub-structure can serve as an excellent plasmonic sensor with a sensitivity of $\sim$820 nm/RIU and a figure of merit of $\sim 3.2 \times 10^5$. The utilization of the anti-symmetric mode in the MIM waveguide provided a new possibility for designing high-performance plasmonic devices.

2. Structure and Simulations

The proposed plasmonic waveguide structure is schematically shown in Fig. 1, which is composed of a MIM structure with two different grooves. This system is a two-dimensional model, and the white and blue parts denote air ($\varepsilon_d = 1.0$) and Ag (ε_m), respectively. The permittivity of Ag is characterized by the Drude model: $\varepsilon_m = \varepsilon_\infty - \omega_p^2/(\omega^2 + i\omega\gamma)$ with $\varepsilon_\infty = 3.7$, $\omega_p = 9.1$ eV. $\gamma = 0.018$ eV [32]. The length and height of the two grooves are L_1, H_1 and L_2, H_2, respectively. The width of the MIM waveguide is w. The transmittance of SPPs is defined as the quotient between the SPP power flows (obtained by integrating the Poynting vector over the channel cross-section) of the observing port with structures (two grooves) and without structures [25], [27].

In order to investigate the optical responses of the proposed structure, its transmission spectra are numerically calculated using the finite element method (FEM) of COMSOL Multiphysics. In the simulations, first perform the boundary mode analysis on the input port of the structure and then solve the wave propagation problem using the mode shape obtained by the first step as a boundary condition. The width of the MIM waveguide is set to be $w = 50$ nm and is fixed throughout the paper. The lengths of the two grooves are set to be $L_1 = 500$ nm, $L_2 = 500$ nm, the height of the low groove is set to be $H_2 = 225$ nm. In this case, the two grooves can be act as a plasmonic resonator, and the calculated transmission spectra are displayed in Fig. 2(a)–(e). Here, $\Delta H = H_1 - H_2$ is to represent the height difference between the two grooves. Obviously, two Fano resonances together with a broad Lorentzian-like profile emerges in each of the

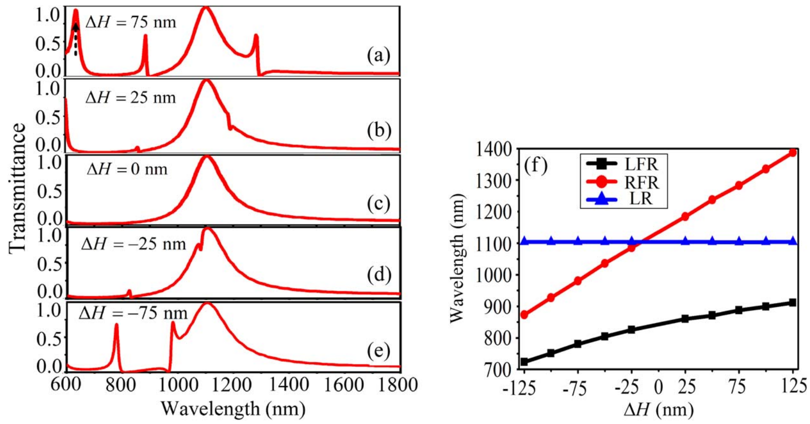

Fig. 2. Transmission spectra of the plasmonic waveguide system for different ΔH of (a) $\Delta H = 75$ nm, (b) $\Delta H = 25$ nm, (c) $\Delta H = 0$ nm, (d) $\Delta H = -25$ nm, and (e) $\Delta H = -75$ nm when $L_1 = 500$ nm, $L_2 = 500$ nm, and $H_2 = 225$ nm. (f) Dependence of the resonant wavelengths on the difference ΔH.

transmission spectra when $\Delta H \neq 0$. When $\Delta H = 0$ nm, only the broad Lorentzian-like profile is observed, as shown in Fig. 2(c), indicating that only the symmetry of the structure is broken, Fano resonances can be emerge. Specifically, when $\Delta H = 75$ nm, another Fano resonance peak appears in the transmission spectrum, as shown in Fig. 2(a) (denoted by the black arrow), and to facilitate the presentation, we call it the new Fano resonance or NFR.

As we know, in a rectangular cavity, the x- and y-directional resonances can be excited. We use mode (m, n) to denote different resonant modes in the rectangular cavity, m, n are integers and indicate the x- and y-directional resonant orders, respectively. In a plasmonic resonator, the accumulated phased shift per round trip for the SPPs is $\Phi = 4\pi n_{eff} S/\lambda + 2\varphi$ [33], [34]. Constructive interference should occur when $\Phi = 2N\pi$, and thus the resonant wavelength is determined by

$$\lambda = \frac{2n_{neff} S}{(N - \varphi/\pi)} \tag{1}$$

where n_{eff} denotes the effective index of the SPPs, which can be obtained by solving the eigenfunction in the MIM waveguide [35]. φ is the phase shift brought by the SPP reflection off the metal wall in the resonator, S presents the L or H $(H_1 + H_2 + w)$ of the rectangular cavity, and $N = 2^{m+n}$. Based on (1), we can obtain that the dependence of the variation of the resonant wavelength on the resonator length S is

$$\frac{d\lambda}{dS} = \frac{2n_{eff}}{N - \varphi/\pi}. \tag{2}$$

In order to understand the underlying physics of the resonant peaks in the transmission spectra, the corresponding field distributions of $|H_z|^2$ at the transmission peaks in the proposed structure with $L_1 = 500$ nm, $L_2 = 500$ nm, $H_2 = 225$ nm, and $\Delta H = 75$ nm are displayed in Fig. 3(a)–(d). Obviously, the four resonant modes can be named mode (1, 0), mode (0, 1), mode (1, 1), and mode (0, 2) for Fig. 3(a)–(d), respectively. First, we begin with the broad Lorentzian resonance or LR mode, which exhibits a nearly symmetric Lorentzian-like profile, as shown in Fig. 2. From Fig. 3(a), it is found that there is no node for the distribution along the y-axis direction for the broad transmission peak at $\lambda = 1103$ nm, yielding a symmetric waveguide mode in the plasmonic resonator. Moreover, its resonant wavelength keeps almost unchanged $(\Delta\lambda/\Delta H \approx 0)$ with the difference ΔH increasing, as shown by the blue symbol line in Fig. 2(f). Because the resonant wavelength of LR is determined by the fixed values of L [33], we find that there is a large distribution proportion of the electromagnetic field at the connecting part between the

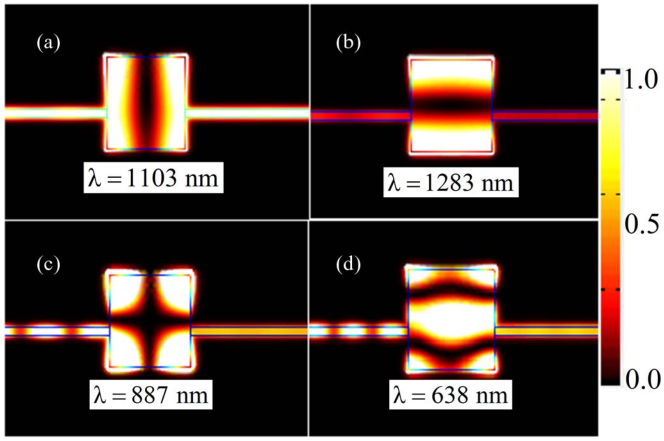

Fig. 3. Field distributions ($|H_z|^2$) at (a) $\lambda = 638$ nm, (b) $\lambda = 1103$ nm, (c) $\lambda = 887$ nm, and (d) $\lambda = 1283$ nm for the proposed structure at $\Delta H = 75$ nm.

plasmonic resonator and the MIM waveguide. Thus, the power flow of the symmetric waveguide mode in the plasmonic resonator can be easily leaked into the MIM waveguide, bringing a large leaky loss for the symmetric waveguide mode. As a result, the symmetric mode results in a broad Lorentzian-like response profile [see Fig. 2(c)], similar to the results in the previous reports [14], [18], [27], [32]–[34].

However, the situation for the left Fano resonance (LFR) or mode (1, 1) becomes different. Increasing ΔH, the resonant wavelengths of LFR has a redshift with a slope of $\Delta\lambda/\Delta H \approx 0.85$, as shown by the black symbol line in Fig. 2(f). Evidently, a standing wave pattern with strong intensities is excited in the plasmonic resonator because of the structural breaking [19]. Moreover, there exists each node for the distribution along the x- and y-axis direction, yielding an anti-symmetric waveguide mode in the plasmonic resonator [31]. In this case, the anti-node is nearly at the connecting part of the plasmonic resonator and the MIM waveguide, as shown in Fig. 3(c). Thus, the power flow of the anti-symmetric waveguide mode in the plasmonic resonator is difficult to leak into the MIM waveguide. That is, the power flow is trapped in the plasmonic resonator. This can result in a strongly trapped resonance in the plasmonic resonator, as shown in Fig. 3(c). Consequently, the interference of the narrow trapped resonance mode (1, 1) and the broad Lorentzian-like resonance mode (1, 0), which are based on different waveguide modes in the plasmonic resonator, gives rise to the Fano profile in the transmission spectra [1], [2], [14], [25], as shown in Fig. 2. For the mode (1, 1), the effective cavity length is $L + H$, and simulations show that φ equals about π. Thus, based on (2), it is easy to get that $d\lambda/dH \approx 2 \times 0.64/(4 - \pi/\pi) \times (1 + H/L) \approx 0.85$. These results agree well with the slope of the black symbol line in Fig. 2(f).

For the right Fano resonance (RFR) or mode (0, 1), it is also redshift with a slope $\Delta\lambda/\Delta H \approx 2$ when the height of the resonator increases, as shown in the red symbol line in Fig. 2(f). In this case, the antinodes of the standing wave pattern appear on both up and bottom edges of the resonator. Thus, the power flow of this waveguide mode in the plasmonic resonator is difficult to leak into the MIM waveguide. That is, the power flow is trapped in the plasmonic resonator. This can result in a strongly trapped resonance in the plasmonic resonator, as shown in Fig. 3(b). Consequently, the interference of the narrow trapped resonance mode (0, 1) and the broad Lorentzian-like resonance mode (1, 0), which are based on different waveguide modes in the plasmonic resonator, gives rise to the Fano profile in the transmission spectra [1], [2], [14], [25], as shown in Fig. 2. For the mode (0, 1), we have $S = H$, $N = 2^{0+1} = 2$. Thus, the (2) becomes $d\lambda/dH \approx 2 \times 1/(2 - \pi/\pi) \times (H/H) = 2$, agreeing well with the slope of the red symbol line in Fig. 2(f). According to above analysis, we know that the new Fano resonance (NFR) originates from the interference between the mode (1, 0) and the mode (0, 2).

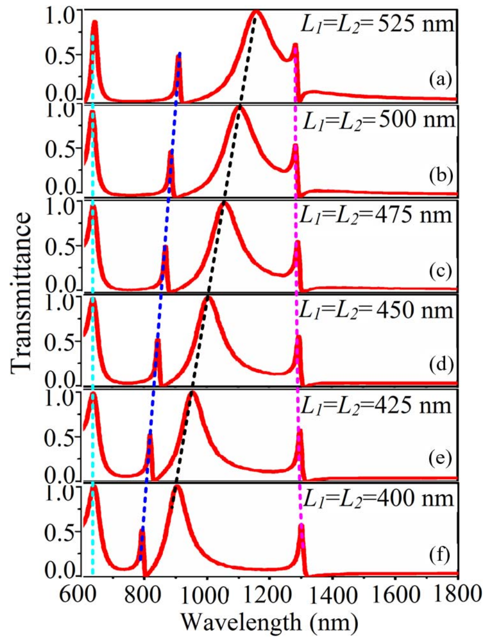

Fig. 4. Transmission spectra for different resonator length of (a) $L_1 = L_2 = 525$ nm, (b) $L_1 = L_2 = 500$ nm, (c) $L_1 = L_2 = 475$ nm, (d) $L_1 = L_2 = 450$ nm, (e) $L_1 = L_2 = 425$ nm, and (f) $L_1 = L_2 = 400$ nm when $H_1 = 300$ nm, and $H_2 = 225$ nm.

To further test our analysis, the transmission spectra of the broken plasmonic resonator are calculated by varying L_1 and L_2, simultaneously, when $H_1 = 300$ nm, $H_2 = 225$ nm, and the results are displayed in Fig. 4. In this case, the height of the plasmonic resonator $H = H_1 + H_2$ is fixed. It is observed the new Fano resonance and right Fano resonance are hardly carried because their resonant wavelengths are determined by the fixed values of H [33], as shown by the green and purple dotted lines in Fig. 4. For the left Fano resonance or mode (1, 1), we know that its resonant wavelength is determined by the values of H and L, and they have the same influence on it. Therefore, for a fixed L or H, the resonant wavelength of LFR has the similar change rule, as shown by the black symbol line in Fig. 2(f) and the blue dotted line in Fig. 4. For the Lorentzian resonance, it is observed that its resonant wavelength is linearly redshifted with increasing length L with a slope of $\Delta\lambda/\Delta L \approx 2$, as shown by the black dotted line in Fig. 4. This linear dependence between the resonant wavelength and the length of the resonator agrees well with the results in the literature [33], [34], as well as (2).

3. Sensing Applications Based on Fano Resonances

Because of the strongly trapped resonance, the Fano resonance exhibits sharp asymmetric profile, where the transmittance can drop or increase sharply from the peak (valley) to the valley (peak) of the spectra. Such a short wavelength change can provide a high sensitivity of spectrum response to the index variations of nearby or surrounding medium for the structure. Therefore, the insulator with different refractive index is employed to investigate the spectral response. The length of the two grooves are fixed to be $L_1 = 500$ nm, $L_2 = 500$ nm, $H_2 = 225$ nm. The transmission spectra are shown in Fig. 5(a) for $\Delta H = -75$ nm and Fig. 5(c) for $\Delta H = 75$ nm, respectively. The resonant wavelength has a red shift when increasing the refractive index. The sensitivity of a sensor (nm/RIU) is usually defined as the shift in the resonance wavelength per unit variations of the refractive index [36]. Thus, the sensitivity of the proposed structure is 680 nm/RIU, 820 nm/RIU and 840 nm/RIU, 1100 nm/RIU for the LFR and RFR at $\Delta H = -75$ nm and $\Delta H = 75$ nm, respectively. That is because the strong field confinement and low leaky loss in our structure [see Fig. 3(b) and (c)], making it more sensitive to the

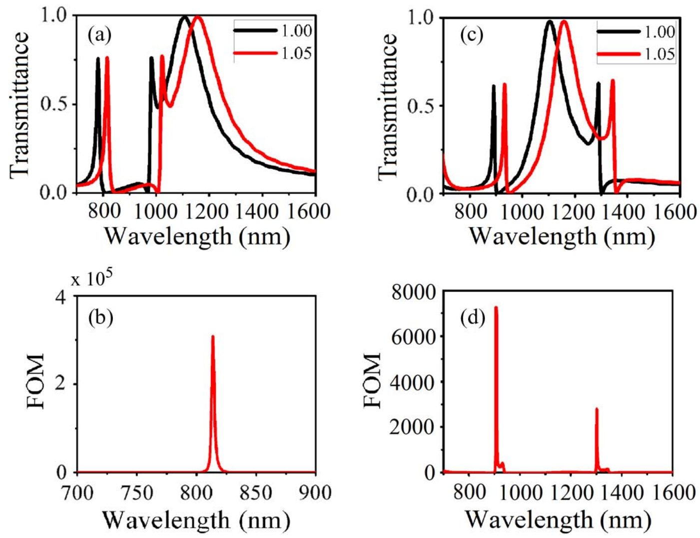

Fig. 5. Transmission spectra for different refractive index at (a) $\Delta H = -75$ nm, and (c) $\Delta H = 75$ nm. The calculated FOM at different wavelength for (b) $\Delta H = -75$ nm, and (d) $\Delta H = 75$ nm. The other parameters are fixed to be $L_1 = 500$ nm, $L_2 = 500$ nm, and $H_2 = 225$ nm.

refractive index of the material. These results are higher than those in the [18], [37]. To better evaluate the performance of the plasmonic sensor, the figure of merit (FOM) is studied, which defined as $\mathrm{FOM} = \Delta T/(T\Delta n)$ [15], [38], [39], where T denotes the transmittance in the proposed structure. The calculated FOM for $\Delta H = -75$ nm and $\Delta H = 75$ nm are displayed in Fig. 5(b) and (d), respectively. The values of FOM is as high as 3.2×10^5 at $\lambda = 820$ nm when $\Delta H = -75$ nm (7400 at $\lambda = 900$ nm when $\Delta H = 75$ nm), which is due to the sharp asymmetric Fano line shape with ultra-low transmittance at this wavelength. These FOM values are significantly greater than that in the previous reports [18], [38].

Although, our structure is similar to that in [23], the parameters of our structure are very different with those in [23]. Many new phenomena emerge due to these differences. For example, the emerging of the anti-symmetric waveguide mode, which can be reflected back and forth off the right and left, up and bottom walls in the plasmonic resonator, constructing two Fabry–Perot resonators [14], [27], [40], makes our structure more functional in devices.

4. Conclusion

In summary, by utilizing the anti-symmetric waveguide mode in the MIM waveguide structure, an asymmetric plasmonic resonator was proposed to achieve multiple Fano resonances. The asymmetrical line shape and the resonant wavelength can be easily tuned by changing the geometrical parameters of the structure. Simulation results show that by introducing a small structural breaking in the plasmonic resonator, both symmetric and anti-symmetric waveguide modes can be excited. The interaction of the symmetric and anti-symmetric waveguide modes gives rise to the Fano resonances in the plasmonic system. These multiple Fano resonances resulted from different mechanisms and thus had different responses to the variations of the structural dimensions. A nano-sensor was designed based on the sharp asymmetrical profiles, which yielded a sensitivity of $\sim$820 nm/RIU and a figure of merit of $\sim 3.2 \times 10^5$. The utilization of the anti-symmetric mode in the MIM waveguide provided a new possibility for designing high-performance plasmonic devices.

References

[1] B. Luk'yanchuk *et al.*, "The Fano resonance in plasmonic nanostructures and metamaterials," *Nat. Mater.* vol. 9, no. 9, pp. 707–715, Sep. 2010.

[2] A. Miroshnichenko, S. Flach, and Y. Kivshar, “Fano resonances in nanoscale structures,” *Rev. Mod. Phys.* vol. 82, no. 3, pp. 2257–2298, Aug. 2010.
[3] A. D. Khan and G. Miano, “Plasmonic Fano resonances in single-layer gold conical nanoshells,” *Plasmonics*, vol. 8, no. 3, pp. 1429–1437, Sep. 2013.
[4] S. Mukherjee *et al.*, “Fanoshells: Nanoparticles with built-in Fano resonances,” *Nano Lett.*, vol. 10, no. 7, pp. 2694–2701, May 2010.
[5] O. Pena-Rodriguez, A. Rivera, M. Campoy-Quiles, and U. Pal, “Tunable Fano resonance in symmetric multilayered gold nanoshells,” *Nanoscale*, vol. 5, no. 1, pp. 209–216, Aug. 2012.
[6] J. Shu, W. Gao, and Q. Xu, “Fano resonance in concentric ring apertures,” *Opt. Exp.*, vol. 21, no. 9, pp. 11 101–11 106, May 2013.
[7] A. Cetin and H. Altug, “Fano resonant ring/disk plasmonic nanocavities on conducting substrates for advanced biosensing,” *ACS Nano*, vol. 6, no. 11, pp. 9989–9995, Aug. 2012.
[8] Y. H. Fu, J. B. Zhang, Y. F. Yu, and B. Luk'yanchuk, “Generating and manipulating higher order Fano resonances in dual-disk ring plasmonic nanostructures,” *ACS Nano*, vol. 6, no. 6, pp. 5130–5137, Jun. 2012.
[9] Y. Zhang, T. Jia, H. Zhang, and Z. Xu, “Fano resonances in disk-ring plasmonic nanostructure: Strong interaction between bright dipolar and dark multipolar mode,” *Opt. Lett.*, vol. 37, no. 23, pp. 4919–4921, Dec. 2012.
[10] L. V. Brown, H. Sobhani, J. B. Lassiter, P. Nordlander, and N. J. Halas, “Heterodimers: Plasmonic properties of mismatched nanoparticle pairs,” *ACS Nano*, vol. 4, no. 2, pp. 819–832, Feb. 2010.
[11] J. Wang *et al.*, “Double Fano resonances due to interplay of electric and magnetic plasmon modes in planar plasmonic structure with high sensing sensitivity,” *Opt. Exp.*, vol. 21, no. 2, pp. 2236–2244, Jan. 2013.
[12] J. A. Fan *et al.*, “Fano-like interference in self-assembled plasmonic quadrumer clusters,” *Nano Lett.*, vol. 10, no. 11, pp. 4680–4685, Aug. 2010.
[13] N. A. Mirin, K. Bao, and P. Nordlander, “Fano resonances in plasmonic nanoparticle aggregates,” *J. Phys. Chem. A*, vol. 113, no. 16, pp. 4028–4034, Apr. 2009.
[14] J. J. Chen, Z. Li, J. Li, and Q. H. Gong, “Compact and high-resolution plasmonic wavelength demultiplexers based on Fano interference,” *Opt. Exp.*, vol. 19, no. 10, pp. 9976–9985, May 2011.
[15] J. J. Chen *et al.*, “Coupled-resonator-induced Fano resonances for plasmonic sensing with ultra-high figure of merits,” *Plasmonics*, vol. 8, no. 4, pp. 1627–1632, Dec. 2013.
[16] X. J. Piao, S. Yu, S. Koo, K. Lee, and N. Park, “Fano-type spectral asymmetry and its control for plasmonic metal–insulator–metal stub structures,” *Opt. Exp.*, vol. 19, no. 11, pp. 10 907–10 912, May 2011.
[17] J. J. Chen *et al.*, “Response line-shapes in compact coupled plasmonic resonator systems,” *Plasmonics*, vol. 8, no. 2, pp. 1129–1134, Jun. 2013.
[18] H. Lu, X. M. Liu, D. Mao, and G. X. Wang, “Plasmonic nanosensor based on Fano resonance in waveguide-coupled resonators,” *Opt. Lett.* vol. 37, no. 18, pp. 3780–3782, Sep. 2012.
[19] V. A. Fedotov, M. Rose, S. L. Prosvirnin, N. Papasimakis, and N. I. Zheludev, “Sharp trapped-mode resonances in planar metamaterials with a broken structural symmetry,” *Phys. Rev. Lett.*, vol. 99, no. 14, Oct. 2007, Art. ID. 147401.
[20] A. Artar, A. A. Yanik, and H. Altug, “Multispectral plasmon induced transparency in coupled meta-atoms,” *Nano Lett.*, vol. 11, no. 4, pp. 1685–1689, Apr. 2011.
[21] A. Artar, A. A. Yanik, and H. Altug, “Directional double Fano resonances in plasmonic hetero-oligomers,” *Nano Lett.*, vol. 11, no. 9, pp. 3694–3700, Sep. 2011.
[22] D. Wang, X. Yu, and Q. Yu, “Tuning multiple Fano and plasmon resonances in rectangle grid quasi-3D plasmonic-photonic nanostructures,” *Appl. Phys. Lett.*, vol. 103, no. 5, Jul. 2013, Art. ID. 053117.
[23] J. W. Qi *et al.*, “Independently tunable double Fano resonances in asymmetric MIM waveguide structure,” *Opt. Exp.*, vol. 22, no. 12, pp. 14 688–14 695, Jun. 2014.
[24] T. Xu, Y. K. Wu, X. G. Luo, and L. J. Guo, “Plasmonic nanoresonators for high-resolution colour filtering and spectral imaging,” *Nat. Commun.*, vol. 24, no. 1, p. 59, Aug. 2010.
[25] J. J. Chen *et al.*, “Plasmonic Y-splitters of high wavelength resolution based on strongly coupled-resonator effects,” *Plasmonics,* vol. 7, no. 3, pp. 441–445, Sep. 2012.
[26] K. H. Wen *et al.*, “Electromagnetically induced transparency-like transmission in a compact side-coupled T-shaped resonator,” *J. Lightw. Technol.*, vol. 32, no. 9, pp. 1071–1707, May 2014.
[27] J. J. Chen, C. Wang, R. Zhang, and J. H. Xiao, “Multiple plasmon-induced transparencies in coupled-resonator systems,” *Opt. Lett.* vol. 37, no. 24, pp. 5133–5135, Dec. 2012.
[28] J. A. Dionne, L. A. Sweatlock, M. T. Sheldon, A. P. Alivisatos, and H. A. Atwater, “Silicon-based plasmonics for on-chip photonics,” *IEEE J. Sel. Topics Quantum*, vol. 16, no. 1, pp. 295–306, Jan. 2010.
[29] E. Feigenbaum and H. A. Atwater, “Resonant guided wave networks,” *Phys. Rev. Lett.*, vol. 104, no. 14, Apr. 2010, Art. ID. 147402.
[30] S. B. Raghunathan *et al.*, “Plasmon switching: Observation of dynamic surface plasmon steering by selective mode excitation in a sub-wavelength slit,” *Opt. Exp.*, vol. 20, no. 14, pp. 15 326–15 335, Jul. 2012.
[31] Z. Chen, J. J. Chen, L. Yu, and J. H. Xiao, “Sharp trapped resonances by exciting the anti-symmetric waveguide mode in a metal–insulator–metal resonator,” *Plasmonics*, Aug. 2014, doi: 10.1007/s11468-014-9786-0.
[32] X. S. Lin and X. G. Huang, “Tooth-shaped plasmonic waveguide filters with nanometeric sizes,” *Opt. Lett.* vol. 33, no. 23, pp. 2874–2876, Dec. 2008.
[33] Z. P. Zhou, F. F. Hu, and H. X. Yi, “Wavelength demultiplexing structure based on arrayed plasmonic slot cavities,” *Opt. Lett.* vol. 36, no. 8, pp. 1500–1502, Apr. 2011.
[34] Q. Zhang, X. G. Huang, X. S. Lin, J. Tao, and X. P. Jin, “A subwavelength coupler-type MIM optical filter,” *Opt. Exp.*, vol. 17, no. 9, pp. 7549–7554, Apr. 2009.
[35] J. A. Dionne, L. A. Sweatlock, and H. A. Atwater, “Plasmon slot waveguides: Towards chip-scale propagation with subwavelength-scale localization,” *Phys. Rev. B*, vol. 73, no. 3, Jan. 2006, Art. ID. 035403.
[36] N. Liu, M. Mesch, T. Weiss, M. Hentschel, and H. Giessen, “Infrared perfect absorber and its application as plasmonic sensor,” *Nano Lett.*, vol. 10, no. 7, pp. 2342–2348, Jul. 2010.

[37] N. Liu *et al.*, “Planar metamaterial analogue of electromagnetically induced transparency for plasmonic sensing,” *Nano Lett.*, vol. 10, no. 4, pp. 1103–1107, Apr. 2010.
[38] J. Becker, A. Trugler, A. Jakab, U. Hohenester, and C. Sonnichsen, “The optimal aspect ratio of gold nanorods for plasmonic bio-sensing,” *Plasmonics*, vol. 5, no. 2, pp. 161–167, Jun. 2010.
[39] R. Ameling *et al.*, “Cavity-enhanced localized plasmon resonance sensing,” *Appl. Phys. Lett.*, vol. 97, no. 25, Dec. 2010, Art. ID. 253116.
[40] J. J. Chen, Z. Li, X. Zhang, J. H. Xiao, and Q. H. Gong, “Submicron bidirectional all-optical plasmonic switches,” *Sci. Rep.*, vol. 3, p. 1541, Mar. 2013.